43rd AIAA Aerospace Sciences Meeting and Exhibit
10 - 13 Jan 2005

AIAA Paper 2005-0515

High Repetition Rate Planar Velocity Measurements in a Mach 2.0 Compressible Axisymmetric Jet

Brian S. Thurow*, Marc Blohm†, Walter R. Lempert‡ and Mo Samimy§
The Ohio State University, Gas Dynamics and Turbulence Laboratory
2300 West Case Road, Columbus, OH 43235

The convective velocity of large-scale structures in a Mach 2.0 compressible axisymmetric jet is explored using both qualitative flow visualization and quantitative velocity data acquired using MHz rate planar Doppler velocimetry. Space-time correlations based on qualitative flow visualization image sequences appear to show two modes of convective velocity, a fast and a slow mode, that deviate significantly from the theoretically expected value. Space-time correlations based on velocity data, however, appear to show only a single mode of convective velocity with a magnitude close the theoretical value. It is found that the use of space-time correlations on inherently qualitative flow visualization images can produce misleading results. The implications of these findings are significant with further work necessary before broader conclusions can be drawn.

I. Introduction

COMPRESSIBLE free shear layers are encountered in a wide variety of modern applications. Some examples include the base flow behind a missile, the separated flow of a stalled airfoil and the noise producing high-speed exhaust of a jet engine. With the development of faster modes of transportation and the next generation space launch vehicle, our understanding of compressible free shear layers will become even more important. For example, the development of SCRAMJET engines is partially hindered by the lack of ability to rapidly mix fuel with the air flowing through the engine. The long times necessary to achieve mixing necessitate the use of long (and heavy) combustion chambers, reducing efficiency of this next generation engine. Thus, formulating a better understanding of compressible free shear layers, which could lead to effective mixing enhancement schemes, is quite important to the fluid dynamics community.

Over the last couple of decades, the study of compressible free shear layers has largely revolved around the concept of the convective Mach number, M_c, first introduced in the numerical work of Bogdanoff [1983] and later in the experimental work of Papamoschou and Roshko [1988]. In these works, it was found that this parameter is effective in characterizing the growth rate of planar shear layers. Physically, the convective Mach number represents the velocity of a large-scale structure in the shear layer with respect to either the fast or slow-speed streams. For two pressure-matched parallel streams with equal specific heat ratios the convective Mach number and convective velocity are given as:

$$M_c = \frac{U_1 - U_2}{a_1 + a_2} = \frac{U_1 - U_{c,i}}{a_1} = \frac{U_{c,i} - U_2}{a_2} \tag{1.1}$$

$$U_{c,i} = \frac{a_1 U_2 + a_2 U_1}{a_1 + a_2} \tag{1.2}$$

where U_1 and U_2 are the high- and low-speed free stream velocities, a_1 and a_2 are the speeds of sound and $U_{c,i}$ is the theoretical isentropic convective velocity.

The validity of the physical concept behind the convective Mach number has been investigated by several researchers through experimental measurements of the convective velocity of large-scale structures. Fourgette et al.

---

* Now an Assistant Professor with Auburn University, Aerospace Engineering Department, 211 Aerospace Engineering Building, Auburn, AL 36849-5338, (334) 844-6827, **thurobs@eng.auburn.edu**, AIAA Member
† Graduate Student, AIAA Student Member
‡ Professor, Associate Fellow AIAA
§ Professor, Associate Fellow AIAA

[1991], Mahadevan et al. [1995], Poggie and Smits [1996], Papamoschou and Bunyajitradulya [1997], Smith and Dutton [1999], Murakami and Papamoschou [2000] and Thurow et al. [2002, 2003] used time-correlated sequences of planar light-scattering flow visualization images (typically only a pair of time-correlated images could be obtained) and two-dimensional space-time cross-correlation algorithms to compute the convective velocity of structures. Samimy et al. [1992] and Elliott et al. [1995] also used time-correlated flow visualization images, but computed the convective velocity using a one-dimensional space-time correlation. Hall et al. [1993] and Rossman et al. [2000] calculated convective velocities based on shocks emitted from the shear layer and observed in schlieren images. In addition, Lepicovsky et al. [1987] and Crawford and Elliott [1999] calculated the phase velocity of large-scale structures in excited supersonic jets using phase averaged schlieren and planar flow visualization images respectively.

With the exception of the works by Samimy et al. [1992] and Elliott et al. [1995], which found a large dependence of the convective velocity on transverse location, a common result of all these studies independent of measurement technique is that the convective velocity deviates substantially from that predicted by Equation 1.2. This deviation takes the form of either a 'fast' mode or a 'slow' mode depending on the conditions of the experiment. A clear physical explanation for these modes has not been discovered, but their presence has motivated some discussions in the literature about their origin, including, for example, the speculation on the presence of shocks (or shocklets) within the mixing layer [e.g. Hall et al., 1993 and Papamoschou, 1994]. In addition, Thurow et al. [2003] detected the simultaneous presence of both a 'fast' and a 'slow' mode in a Mach 2.06 axisymmetric jet, a unique measurement that further complicated the understanding of convective velocity in compressible free shear layers.

The deviation of the convective velocity from theory is revisited in this work through the application of a recently developed experimental technique, MHz rate planar Doppler velocimetry, to a Mach 2.0 axisymmetric jet. This technique allows for the acquisition of a sequence of 28 time-correlated frames of planar velocity data. Space-time correlations are used to track structures as they convect downstream and thus determine a convective velocity. Space-time correlations based on both flow visualization and velocity data of the Mach 2.0 jet are used to determine the convective velocity of large-scale structures within the M_c=0.87 shear layer. As will be discussed in detail, convective velocity measurements based on velocity data are dramatically different than those based on flow visualization images.

II. Experimental Methods

A. Experimental Facility

All experiments were conducted in the free jet facility located at The Ohio State University's Gas Dynamics and Turbulence Laboratory (GDTL). The facility consists of a jet stand and stagnation chamber to which a variety of nozzles may be attached. Air is supplied from two four-stage compressors; it is filtered, dried and stored in two cylindrical tanks with a total capacity of 42.5 m^3 at 16.5 MPa (1600 ft^3 at 2500 psi). The stagnation chamber contains a perforated plate and two screens of varying porosity to condition the flow to be as uniform as possible prior to entering the nozzle. More details concerning the facility can be found in Hileman and Samimy [2001] and Kerechanin et al. [2001].

Pressure in the stagnation chamber is controlled through the actuation of one of two Fisher control valves, arranged in parallel, with each configured for either low or high mass flow rate conditions. Actuation is automatic through the use of a Fisher-Rosemount PID-based process controller (Model DPR 960), which measures the stagnation pressure via an attached pressure transducer and adjusts the valve accordingly. Constant pressure can be maintained with an accuracy of approximately +/- 0.5%. The nozzle discussed in this study had a design Mach numbers of 2.0 and an exit diameter of 25.4 mm (1"). It is a cold flow with a stagnation temperature of approximately 300 K. The diverging portion of the nozzle was designed using the method of characteristics for uniform flow at the nozzle exit. The Mach number was experimentally determined using a pitot probe to be 2.06, with an associated Reynolds numbers based on nozzle diameter of 2.6 x 10^6.

B. Experimental Techniques: MHz Rate Flow Visualization and Planar Doppler Velocimetry

The main experimental technique employed in this work is MHz rate planar Doppler velocimetry (PDV). MHz rate PDV is a recently developed technique and utilizes a home-built pulse burst laser system, two ultra-high framing rate cameras and a molecular vapor filter. In this work, MHz rate PDV was used to acquire both flow visualization and velocity images, eliminating the need for two separate experimental set-ups and runs. For the sake

of brevity, only a brief description of the technique and equipment are provided here with the reader referred to Thurow [2005] for more details.

Planar Doppler Velocimetry (PDV) is a powerful optical diagnostic technique that can be used to measure all three components of instantaneous velocity over a two-dimensional plane with high spatial resolution. PDV accomplishes this task by measuring the Doppler shift in frequency of light scattered by moving particles in the flow field. The relatively small frequency shift is discriminated using an atomic or molecular vapor filter. The Doppler shift, Δf_d, is related to the fluid velocity by the simple expression,

$$\Delta f_d = \frac{(\vec{s} - \vec{o})}{\lambda} \cdot \vec{V} \tag{2.1}$$

where $\vec{s}$ is the unit vector in the direction of the scattered light, $\vec{o}$ is the unit vector in the direction of the incident laser light, λ is the wavelength of the light and $\vec{V}$ is the velocity vector of the flow.

A typical one-component PDV system utilizes a pulsed injection-seeded Nd:YAG laser, one or two scientific grade CCD cameras and a molecular iodine filter. The laser is used to illuminate a plane of the flow with narrow spectral linewidth light. The Doppler shifted scattered light is then split into two paths, a signal path and a reference path, using a beam splitter and imaged onto the camera(s). In this manner the absolute absorption of scattered light, as it passes through an iodine cell placed in one of the beam paths, is measured at every spatial location within the object plane. For scattering by relatively large (as compared to molecular dimension) particles, this absorption is a function of particle velocity only. Accurate calibration and image mapping algorithms have been developed with the result that velocity accuracies of ~1-2 m/s are now achievable. More details concerning the history of PDV, the art of its application and recent advances can be found in comprehensive review articles by Elliott and Beutner [1999] and Samimy and Wernet [2000].

Typical PDV systems are limited by commercially available lasers and cameras to repetition rates on the order of 10-100 Hz. Repetition rates on the order of 1 MHz are achieved through the use of a home-built pulse burst laser system and two ultra-high frame rate cameras. The pulse burst laser system is an Nd:YAG based laser with the ability to produce a burst of 1 – 99 short duration (10 nsec), high energy (order of 10 mJ/pulse) pulses over a timespan of approximately 100 microseconds with repetition rates as high as 1 MHz. The pulse burst laser system is discussed extensively in Thurow et al. [2004]. The two cameras used in this study were manufactured by Princeton Scientific Instruments and have the ability to capture a sequence of 28 images at up to 1 million frames per second (1 MHz). High frame rates are achieved by shifting charge produced on the active area of the chip to an array of individual memory modules contained next to each pixel location. When incorporated into a common PDV configuration, the pulse burst laser and high-speed cameras allow for the acquisition of planar velocity data at MHz rates with accuracies on the order of 10 – 20 m/s. The development of this technique is the subject of Thurow et al. [2005].

For the experiments described herein, the laser sheet propagates in the upstream direction at an 18º angle relative to the jet axis. This results in a one component PDV system with sensitivity to velocities in the 0.67 i - 0.22 j + 0.71 k direction, where i is the unit vector in the streamwise direction, j in the transverse direction and k is the out-of-plane unit vector. Although this appears to be a rather odd direction, it should be noted that in the supersonic jets studied here, the streamwise (**u**, i) component of velocity will be an order of magnitude higher than the other velocity components (**v**, j and **w**, k), thus making this measurement predominantly sensitive to the streamwise velocity. Experiments conducted with the laser sheet propagating at a shallower angle produced severe aero-optic aberrations within the laser sheet and could not produce reliable measurements. To validate these measurements, a two component MHz rate PDV experiment was conducted that allowed for a measurement of **u** directly and showed similar results to those presented here. Two component MHz rate PDV was not used for the current experiments due to its decreased field-of-view, increased complexity and decreased accuracy.

In addition to velocity data, flow visualization data was also acquired. Flow visualization images are inherently acquired in the PDV acquisition process. The reference (unfiltered) image is unaffected by the velocity of light scattering particles in the flow and, for all intensive purposes, identical to an image acquired using a flow visualization technique. This unique aspect of PDV allows for the simultaneous acquisition of flow visualization and velocity images without the need for multiple experimental set-ups or runs. Thus, all of the data presented here was obtained during a single experimental run.

C. Particle Seeding Considerations

An important detail about PDV (as well as numerous other techniques) is the requirement for the flow to contain light-scattering particles. For flow visualization, particle seeding is provided via product formation. Product formation is a natural method of seeding where moisture contained in the ambient air condenses as it is entrained

and mixed with the cold, dry jet air. In this manner, particles will only be produced in regions of the mixing layer where intense mixing has occurred, cold temperatures exist and enough time has passed for significant condensation of moisture to occur. Intense mixing is generally associated with large-scale turbulence structures, thus product formation is a convenient method for highlighting large-scale structures within the flow. It is important to note, however, that product formation is the result of a complex process that depends on a number of variables including temperature, mixing and time. Thus, the resulting intensity of scattered light does not correlate directly with any flow variable and the presence of structures can only be inferred from the images.

For PDV, seed particles are required throughout the flow field in order to make a full field velocity measurement. As with flow visualization, product formation is used to seed the mixing layer of the jet. Seeding of the jet core is provided by the injection of a small amount of acetone (~0.4% by mass) into the flow ~10 m upstream of the stagnation chamber where it is evaporated and mixed with the air by the time it reaches the nozzle. Upon expansion to supersonic velocities (and associated colder temperatures of ~155 K), the acetone condenses into small particles, thus producing small light-scattering particles similar to those produced via product formation. Although product formation and acetone condensation mark the majority of the flow field, the low-speed periphery of the jet was, unfortunately, not seeded for the data presented here. A method for seeding the low-speed portion of the jet is currently being devised and results will be available shortly. As will be demonstrated in this work, the lack of measurements in the low-speed portion of the jet can have a substantial effect on the space-time correlation results. Thus, this unknown region of the flow must be dealt with carefully. Three approaches are used in this work towards the treatment of unseeded regions of the flow and will be discussed in Section 1.E.

D. Two-Dimensional Space-Time Correlations

A two-dimensional space-time correlation is used to track structures in the flow as they evolve and move downstream. A structure is defined in the first frame and tracked across the remaining frames. This allows for the calculation of large-scale structures' convective velocities as well as their coherent lifetime. The procedure used here is similar to that used by Fourgette et al. [1991], Mahadevan et al. [1995], Poggie and Smits [1996], Papamoschou and Bunyajitradulya [1997], Smith and Dutton [1999], Murakami and Papamoschou [2000] and Thurow et al. [2002, 2003]. This procedure has been used in the past to analyze time-correlated flow visualization data, but has not been used on quantitative data of a flow variable such as velocity. Conceptually, the space-time correlation used here is similar to conventional space-time correlations where data is acquired over time at two points (i.e. two hot-wires or pressure transducers); the distance between the probes can then be varied to produce multiple separations. Data in this study, however, is acquired across a plane and separations can be achieved by looking at different regions of each image. The discussion will begin with a mathematical description of the correlation.

Consider a two-dimensional time varying signal, $F(x,y,t)$, with dimension m x n. The signal is defined as being within an M x N domain and has N_{total} realizations, or measurements, in time. The ensemble average of the temporally fluctuating signal is:

$$\langle F(x,y)\rangle = \frac{1}{N_{total}}\sum_{k=1}^{N_{total}} F_k(x,y,t_k) \tag{2.2}$$

and the fluctuating signal is:

$$F_k'(x,y,t_k) = F_k(x,y,t_k) - \langle F(x,y)\rangle \tag{2.3}$$

The correlation, C, between two instances of the signal is:

$$C_{i,j} = \frac{1}{mn}\sum_{x=1}^{m}\sum_{y=1}^{n} F_i'(x,y,t_i)F_j'(x,y,t_j) \tag{2.4}$$

where higher values of C represent a better degree of correlation. The correlation coefficient, R, is a normalized representation of the correlation and defined as:

$$R_{i,j} = \frac{C_{i,j}}{\sqrt{C_{i,i}C_{j,j}}} \tag{2.5}$$

R takes a value of 1.0 for perfect correlation (i=j) and -1.0 when the two signals are anti-correlated ($F_i'=-F_j'$). For the data considered herein, we are interested in the movement of a portion of the signal (defined as the structure) with time. Thus, the overall domain (M x N) is larger than the feature of interest, F (m x n). One must account for the movement of the feature in time and space by including a Δx and a Δy term:

$$C_{i,j}(\Delta x,\Delta y)=\frac{1}{mn}\sum_{x=1}^{m}\sum_{y=1}^{n}F_i'(x,y,t_i)F_j'(x+\Delta x,y+\Delta y,t_j) \tag{2.6}$$

$$R_{i,j}(\Delta x,\Delta y)=\frac{C_{i,j}(\Delta x,\Delta y)}{\sqrt{C_{i,i}(0,0)C_{j,j}(\Delta x,\Delta y)}} \tag{2.7}$$

The calculation of $R_{1,j}(\Delta x,\Delta y)$, where j represents each successive frame in a given image sequence, reveals the most interesting features of the flow. In the current experiments, F represents either the image intensity (in the case of the flow visualization images) or the velocity (in the case of the PDV data). F_1 is considered the 'template' and is arbitrarily chosen from the first image in each sequence. It represents the structure to be tracked through the remaining frames. The size (m x n) and location (x_o, y_o) of the template is variable and its effect are explored in Thurow [2005]. By definition, $R_{1,1}$ is the auto-correlation and the maximum correlation is equal to 1.0 for $\Delta x = \Delta y = 0$. The maximum correlation in $R_{1,2}$ will be lower than 1.0 and its location (Δx, Δy) represents the new location of the structure at time, $t = t_o + \Delta t$, where Δt is the time separation between consecutive frames in a sequence (4 microseconds in this study). In a likewise fashion, $R_{1,3}$ can be used to find the location of the structure at time, $t = t_o + 2\Delta t$ and so on through all 28 frames. The convective velocity can be calculated accordingly as:

$$U_c=\frac{\Delta x}{\Delta t} \tag{2.8}$$

As there will be 28 values of Δx and Δt for each image sequence, a least squares fit is used to calculate a single convective velocity for the sequence.

The space-time correlation can be calculated both on an instantaneous basis as well as an ensemble average basis. The ensemble average is represented by:

$$\left\langle R_{1,j}\right\rangle=\frac{1}{N_{total}}\sum_{k=1}^{N_{total}}R_{1,j}(x,y,t_k+(j-1)\Delta t) \tag{2.9}$$

where k represents each image sequence and j is used to represent the time separation between frame j and frame 1. Random noise sources, will average out given enough image sequences. Thus, ensemble averaging allows even noisy data (i. e. two-component PDV data) to be analyzed in a useful and accurate fashion.

The data acquired in this study consists of either intensity or velocity data. Within the first frame of each sequence (consisting of 28 frames) a structure is defined as the signal contained within a window of fixed size and location. This then becomes the template with which each additional frame in the sequence is correlated. The template was chosen to be identical in both size and location as the one used in the computations of Thurow et al. [2003]. The window width is 3δ, where δ is the local shear layer thickness as determined from flow visualization images. In addition, results not presented here show the measurements are largely insensitive to the window width. The window height is large enough to encompass the entire transverse extent of the mixing layer. The center location of the template is fixed at 8.0 x/D for the Mach 2.0 jet. This location is approximately 65% of the potential core length and far enough away from the jet exit to expect large structures within the shear layer, yet sufficiently close to allow the structures to evolve without interference from the opposite side of the jet.

E. Treatment of Unseeded Portions of Flow Field

The seeding techniques employed in this study do not seed the entire flow field and it must be determined what effect this will have on the results. For flow visualization, product formation was used for particle seeding as it is a convenient method for highlighting the most dynamic turbulence features of the flow where intense mixing has occurred. As product formation is a complex process, however, it is not possible to correlate the resulting image intensity directly with a flow variable. Large-scale structures are subsequently defined within the images as existing where intense mixing (high image intensity) has occurred. Thus, the lack of seed particles reveals something about the flow, namely, the lack of a large-scale structure.

In contrast, for velocity data, the lack of seed particles does not provide any information about the flow. Rather, it is simply an unmeasured region of the flow field. In the presence of seed particles, the velocity is measured directly. In regions where there are insufficient particles for a measurement, the velocity of flow is unknown. This presents a number of practical problems when the data is to be used for further analysis. We are interested in how the lack of data in the outer regions of the flow may affect the determination of convective velocity. Three approaches are used and described here to treat the unseeded regions of the flow.

The first method is to simply set the velocity of all unseeded regions of the flow to zero. This is an easy method to implement and can easily, albeit wrongly, be interpreted as harmless. Although the unseeded regions of the flow are low-speed relative to the jet core, they may still have significant velocity. In fact, the average velocity at the boundary between seeded and unseeded fluid, based on the PDV data, is ~100 m/s, a significant value. It is also tempting to assume that a value of zero will not contribute to the overall calculation of the correlation coefficient as discussed in Section 2.D. This, however, is not correct as the calculation of the average and fluctuating velocities will be biased by the incorrect value of zero assigned to these regions of the flow and, thus, the fluctuating component will be nonzero. This will be illustrated further in Section III.

The second method circumvents these issues by performing calculations that ignore the unseeded regions of the flow. The calculation of the space-time correlation (Equation 2.2 through 2.7) is essentially a spatial integration of two signals multiplied together. These equations are written in a form where the integration takes place over an m x n rectangular region of the flow, some of which may be unseeded. An alternative approach would be to perform the integration only over the region in space where seed particles are present. By redefining the area of integration, the unseeded regions of the flow would not affect the computation of the space-time correlation. This produces a potential bias, however, as the space-time correlation will preferentially follow the high speed portion of a structure where seed particles are present. Thus, one might expect the convective velocity measurement to be biased towards higher values.

The last approach considered here is to estimate the velocity in the unseeded regions of the flow. An algorithm was developed to extrapolate the velocity of the unseeded flow regions from the known velocities in the seeded region of the flow. Before proceeding, it is necessary to stress that the following procedure is *not an attempt to solve or measure* the velocity of the flow in unseeded regions of the jet. Rather, the procedure's only purpose is to *provide a more meaningful and realistic representation* of the flow field. Any results presented here must be validated through more detailed experiments (currently being conducted) where measurements are possible throughout the entire flow field. The approach detailed here was only taken in an attempt to gain useful information with the data currently available.

Some of the ideas and concepts used in the algorithm are illustrated in Figure 1. The dotted line schematically shows the average transverse velocity profile across a shear layer, which is known to fit well with an error function [Goebel and Dutton, 1990] or hyperbolic tangent [Samimy and Elliott, 1990]. Instantaneously, however, the velocity profile will look quite different, and is schematically represented by the solid line. For most of the flow field, the velocity can be measured directly using PDV. Towards the outer edges of the shear layer, however, flow seeding is inconsistent and measurements cannot be made. This region is indicated by the shaded area and any velocity data in this area is uncertain. The thick solid represents the assumed velocity profile when a value of zero (method 1) is arbitrarily used to represent the region of uncertainty. Clearly, this is unrealistic. In general, one would expect the velocity to decrease to zero at some distance from the jet centerline. Some velocity profiles that might better represent reality are shown by the dashed lines. As the velocity is uncertain in this area, each of these dashed lines represents an equally valid solution and one cannot determine the true solution.

The main idea of the extrapolation algorithm is to fit a curve to the known velocity data and to extrapolate velocity values into the region of uncertainty using this curve fit. Inherently, these extrapolated values are not real and are imprecise. The main suggestion here is that, at the very least, they will be more realistic than arbitrarily setting the velocity to zero or ignoring the region entirely. The function used to fit a curve to the data will have an impact on the results and should be chosen carefully. Physically, the function should take the velocity smoothly from the edge velocity to zero at some reasonable distance away from the jet centerline. Any functions that meet this criteria are possible solutions and equally valid. Six functions are used here and their results will be compared to assess the sensitivity of the space-time correlation to the selection of the curve fit function.

These functions are:

$$f(y) = a_1(1 - \tanh(a_3(y - a_2))) \tag{2.10}$$

$$f(y) = a_1(1 - erf(a_3(y - a_2))) \tag{2.11}$$

$$f(y) = a_1 \exp(-\frac{(y - a_2)^2}{a_3^2}) \tag{2.12}$$

$$f(y) = a_1 \exp(-a_2(y - a_3)) \tag{2.13}$$

$$f(y) = \frac{a_1}{y - a_2} \tag{2.14}$$

$$f(y) = \frac{a_1}{(y - a_2)^2} \tag{2.15}$$

Equations 2.10 and 2.11 use the hyperbolic tangent and error function, respectively, which have been shown to fit the average velocity profile quite well. Equation 2.12 is Gaussian while Eqn. 2.13 is an exponential decay of the velocity to zero. Equations 2.14 and 2.15 are of the 1/y and $1/y^2$ type. All of these functions approach zero as y approaches infinity.

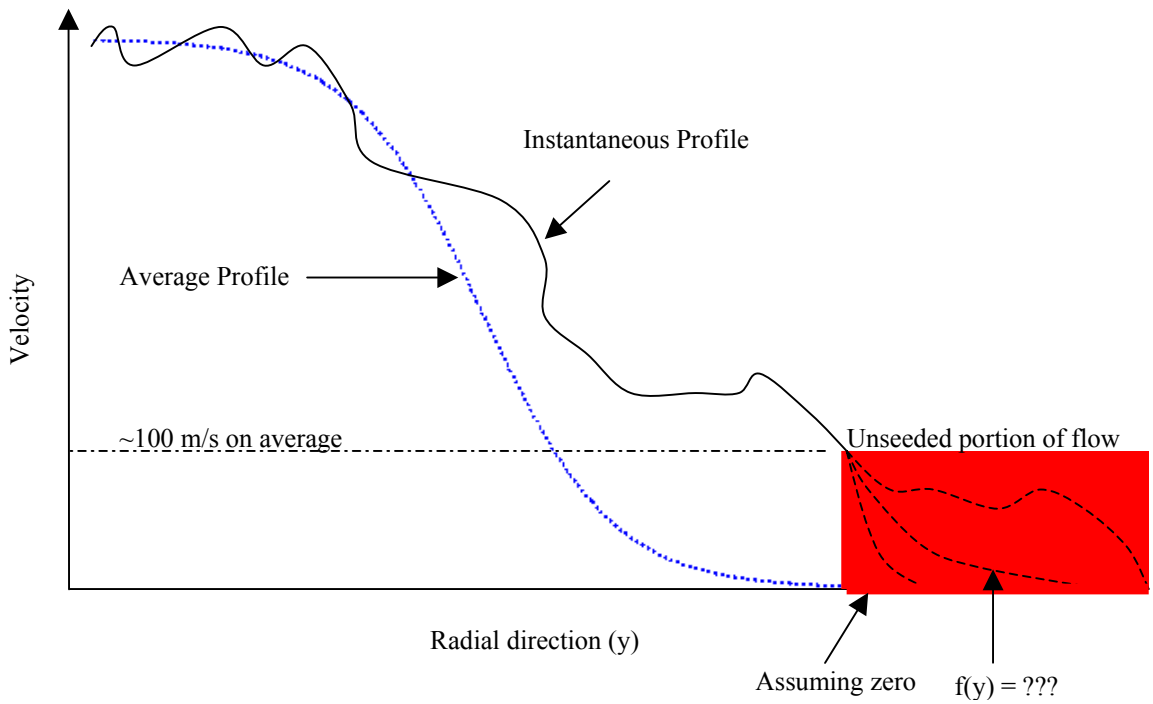

Figure 1 – Schematic demonstrating extrapolation algorithm.

Figure 2 shows an instantaneous velocity profile where the circles indicate measurements obtained using PDV. Note that that the lowest velocity measured in this case is ~80 m/s. The optimally determined curve fits through the data are shown for each function. During curve fitting a constraint is that the velocity must approach zero within a reasonable distance. Just as it is unrealistic to expect the velocity to be zero immediately next to the edge of the mixing layer, it is also unrealistic to expect the velocity to be large at distances far from the jet axis. This condition is imposed by creating additional data points at large values of y (200 pixels, y/D=6) with a velocity of zero. The LDV data of Clancy et al. [1999] shows y/D = 6 to be a reasonable distance to expect the velocity to be close to zero. The method of least squares is used to determine an optimal set of coefficients that produces a function that fits the data, but also is close to zero by y/D=6. In this fashion, the six curve fits also shown in Figure 2 were produced.

Equations 2.10 through 2.12 represent functions with a slope that is zero at $y = a_2$, negative for $y > a_2$ and approaches zero for $y = \infty$. These attributes make these functions ideal for fitting the entire shear layer (i.e. from jet center, y = 0, to ambient, $y = \infty$), which has the same characteristics. For these three functions, the last 20 points of velocity data in each profile are used to determine the optimum curve fit. This causes the tail end of the function to fit the overall shape of the shear layer quite well. Thus, when the overall shear layer is thicker, the tail will be longer and when the shear layer is thin, the tail will be short. Equations 2.13 through 2.15, on the other hand, represent functions with a finite slope that approaches zero only at $y = \infty$. This attribute makes them poor fits for the entire shear layer, but does allow them fit the local shape of the velocity profile near its end. For these functions, only the last 5 points in the velocity profile are used to determine the optimum fit.

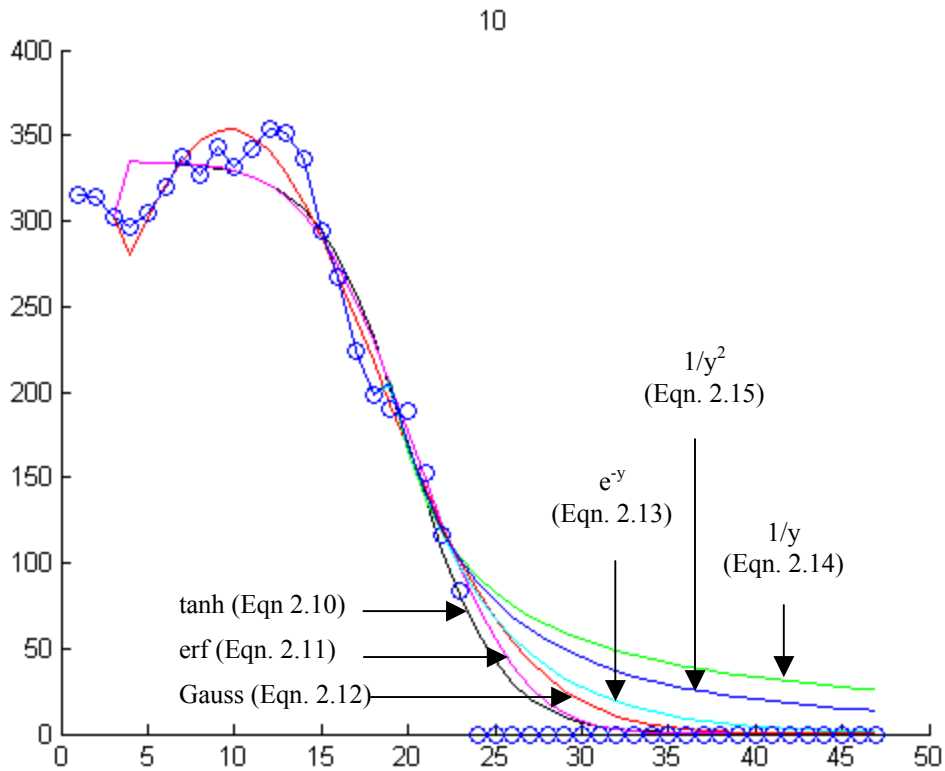

Figure 2 – Curve fits for a sample velocity profile taken from Mach 2.0 jet. Circles represent measured data and lines represent various curve fits through data.

After an optimal set of coefficients has been determined for the velocity profile at each streamwise location in an image, the equations are used to extrapolate the velocity to the unseeded region of the jet. Small scale features in the flow will cause variations in the optimal fit on a column-by-column basis, producing unnatural variations of the velocity in the streamwise direction. In addition, a discontinuity may also occur between the last point of actual data and the beginning of the extrapolated data as the curves are fit through multiple data points. These two problems are corrected through a procedure designed to blend the extrapolated data with the actual data. First, the image is processed with a 5 x 5 low-pass filter to remove any discontinuities and to create a smooth velocity field. After filtering, the velocity data is restored to its original values in locations where measurements seed particles were present. There is one exception. As discussed earlier, the highest uncertainty in velocity occurs at the very edge of the visualized mixing layer where image intensities in the signal and reference images are lowest. Thus, the outermost edges of the velocity data are not restored and the filtered data is used at these locations. This helps create a smoother transition between the measured and extrapolated data, but does not significantly affect the final results.

Figure 3 shows a velocity image before and after application of the extrapolation algorithm using Equation 2.15. All of the originally measured velocity data is intact and unchanged and the vast majority of the image is unaffected. The most notable change is that the boundary between the seeded and unseeded flow is much less distinct and the velocity more smoothly approaches a value of zero for large distances from the jet core. Overall, the largest features of the flow are preserved and the sharp edges between seeded and unseeded fluid eliminated. It is worth repeating that this extrapolation procedure is not intended to provide accurate measurements of flow velocities outside of the mixing layer, but to provide a simple approximation for an otherwise unknown region of the flow. Additional details concerning the extrapolation procedure and its limitations can be found in Thurow [2005].

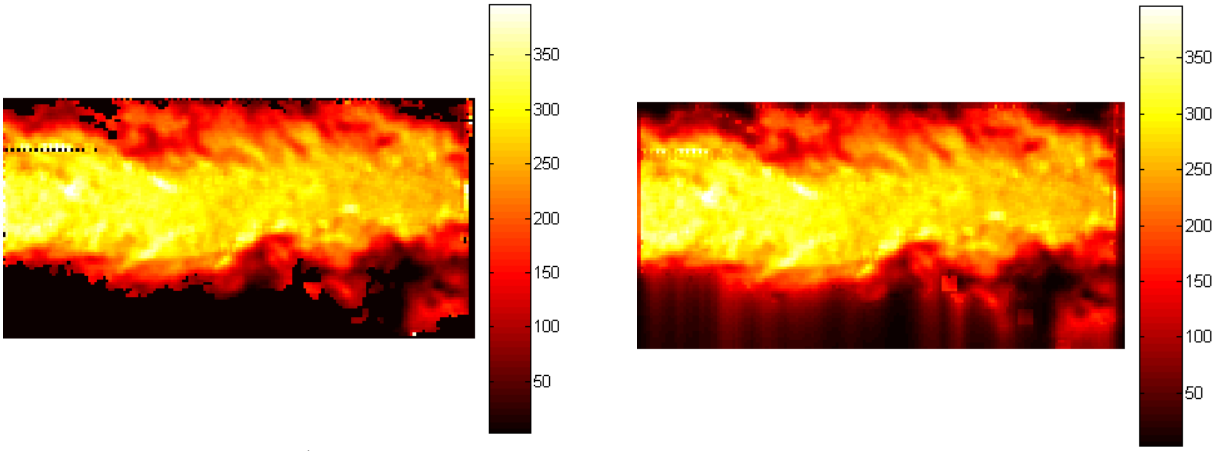

a) b)

Figure 3 – Velocity image a) before and b) after extrapolation of data into unseeded regions of the flow.

III. Experimental Results

A. Mean and Fluctuating Images

Figure 4 is the average intensity and rms intensity fluctuations images of the Mach 2.0 jet without any seeding of the jet core. Only the mixing layer is visualized. The upper half of the mixing layer exhibits a streamwise intensity gradient that is due to the 18º angle of propagation of the laser sheet. The rms intensity fluctuations image shows a distinct trend where peak fluctuations occur on both the upper and lower half of the mixing layer. This is a result of the intermittency of the flow, where the size and location of structures within the mixing layer varies. In the center of the mixing layer, where structures are always present, rms values are quite low. Near the edges of the mixing layer, signal is only present when a structure passes by that location, resulting in high fluctuations in image intensity.

Figure 5 shows the average velocity and rms velocity fluctuations images of the Mach 2.0 jet with velocity values in the unseeded regions of the flow extrapolated using the procedure described earlier. Over 6600 velocity images were used in these calculations. Average velocity values in the jet core are on the order of 340 m/s and are unaffected by the extrapolation procedure. Recalling that the measured velocity is in the 0.67 $\boldsymbol{i}$ - 0.22 $\boldsymbol{j}$ + 0.71 $\boldsymbol{k}$ direction, and assuming that the $\boldsymbol{j}$ and $\boldsymbol{k}$ components of velocity are negligible within the jet core, this corresponds to a jet core velocity of ~507 m/s, which is in excellent agreement with the calculated jet exit velocity of 514 m/s (isentropic, ideal expansion to Mach 2.06). The centerline velocity drops almost linearly with streamwise distance from ~340 m/s at x/D=7 to ~265 m/s (0.67 $\boldsymbol{i}$ - 0.22 $\boldsymbol{j}$ + 0.71 $\boldsymbol{k}$ direction) by 11 x/D.

Within the jet core, velocity fluctuations on the order of 18 m/s, which is ~5% of the jet exit velocity and in general agreement with earlier PDV and LDV studies on Mach 2.0 jets [Clancy et al., 1999]. The rms image shows some artificial noise within the jet core between 7 and 8 x/D. This noise is believed to be similar to and related to damaged CCD pixels immediately above this location. The noise is not a significant concern due to its location within a relatively static portion of the jet. Fluctuations within the lower half of the mixing layer (where the extrapolation algorithm was applied) are on the order of 50 m/s, which is ~15% of the jet exit velocity.

As discussed earlier, three methods were used to treat the unseeded regions of the flow field. These three methods are contrasted in Figures 6 and 7, which show the average and rms fluctuation velocity profiles at x/D = 8.0 for all three cases. When only nonzero values of velocity are considered, the average velocity levels off at ~110 m/s, a reflection of the fact that seed particles only exist where mixing has occurred, and, consequently, the velocity is high. Conversely, if the unseeded region of the flow is assumed to be zero, the velocity profile approaches zero more rapidly. In between these two extremes is the average profile when the extrapolated data is used.

Similar observations are made in the rms velocity fluctuation profiles of Figure 7. There are no differences in, or close to, the jet core because seed particles are always present. With increasing distance from the jet core, however, the velocity fluctuations are quite different for all three methods. The largest fluctuations occur when the velocity in unseeded regions of the jet is set to zero. These fluctuations are expected to be artificially high as the velocity, in many cases, will be much higher than zero, yet the fluctuations are calculated as if they are zero. Conversely, when

the unseeded regions of the jet are not included in the calculations, the fluctuations are lower as measurements are biased to velocities that are 100 m/s or higher.

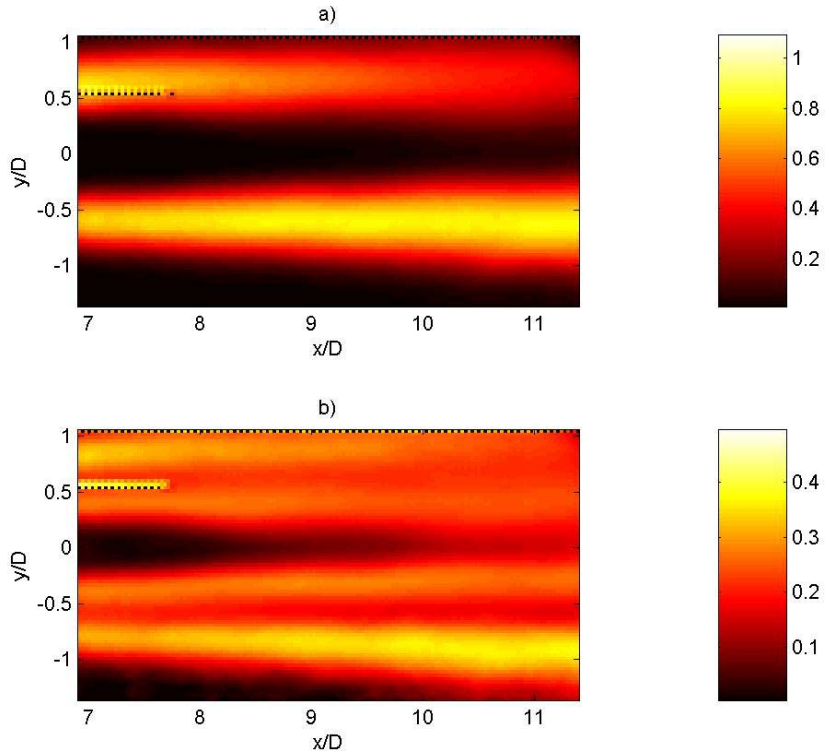

Figure 4: Mach 2.0 flow visualization: a) average intensity and b) rms intensity fluctuations images.

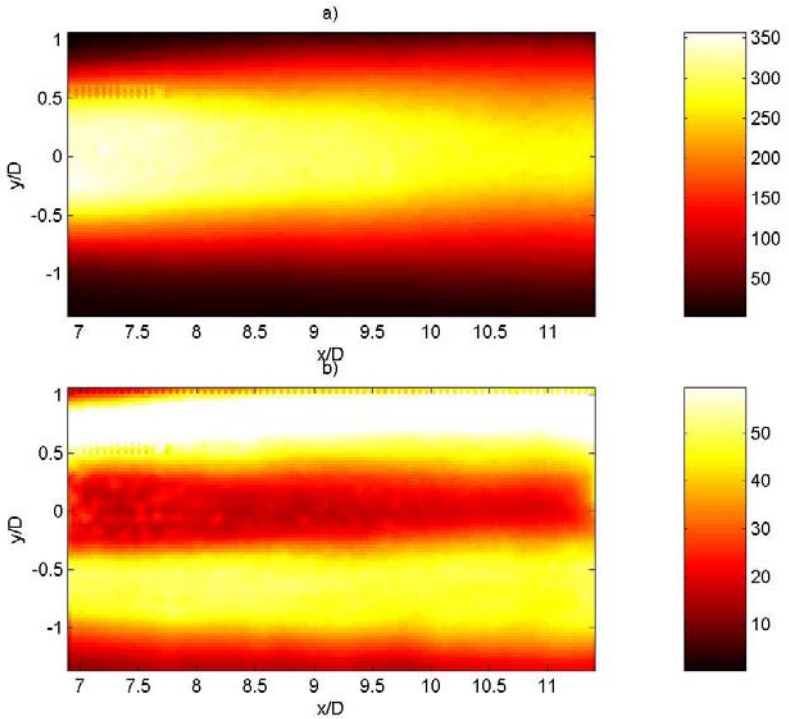

Figure 5: Mach 2.0 velocity data with acetone seeding of the jet core and velocity values extrapolated into unseeded regions: a) average and b) fluctuating velocity images. Only velocity data in the lower half of the mixing layer was extrapolated.

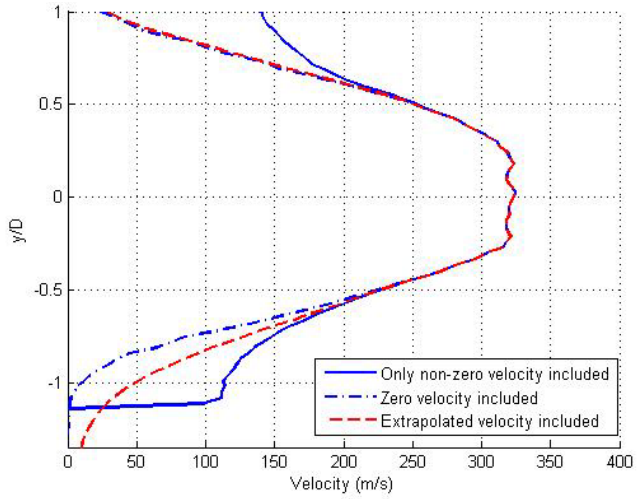

Figure 6: Average velocity profiles at x/D = 8.0. The velocity in unseeded regions of the flow are treated as having zero velocity (solid), not included in the calculations (dash-dot), or extrapolated from actual measurements (dash-dash).

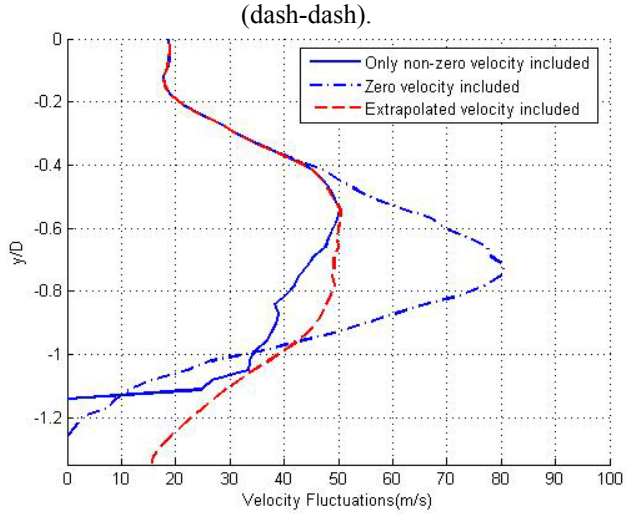

Figure 7: Rms velocity fluctuations profile at x/D = 8.0. The velocity in unseeded regions of the flow are treated as having zero velocity (solid), not included in the calculations (dash-dot), or extrapolated from actual measurements (dash-dash).

The extrapolated data is located approximately in the middle of these two extremes. This is not surprising as the extrapolation algorithm was designed to minimize the biases that result from lacking seed particles in the ambient. Although visually appealing, one cannot say that statistics based on extrapolated data are completely accurate. Only actual measurements throughout the entire flow field will reveal the true nature of this flow. Still, the extrapolated data is an interesting approximation of the flow field that helps provide a glimpse into the physics of the Mach 2.0 jet.

B. Flow Visualization Space-Time Correlations

The space-time correlation data computed in this work is very rich in information, but not very conducive to the print format. In order to present the data in an easy to read format, the following figure consists of four parts, a, b, c and d. Parts a, b and c are produced from the ensemble averaged space-time correlation and Part d) is a compilation of instantaneous measurements. Part a) shows streamwise slices ($\Delta y = 0$) of the spatial correlation of the signal at different instances in time. Part b) is the level of maximum correlation vs. time. Part c) is the streamwise location (Δx) of maximum correlation vs. time and Part d) is a histogram of the peak correlation velocity.

Figure 8 shows the space-time correlation data for the Mach 2.0 flow visualization data. Figure 8 a) is the streamwise slices ($\Delta y = 0$) through the correlation data at several time separations. At t = 0 μs, the peak correlation is 1.0 for $\Delta x = 0$ mm. At t = 32 μs, the correlation has dropped to ~0.6 and is located ~10 mm downstream of the

original location of the structure, an indication of the movement of structures in the flow. At t = 108 μs, the correlation has dropped even further and the distribution has become rather broad. In addition, the spatial correlation appears to have two peaks. Figure 8 c) is an x-t diagram of the streamwise position of maximum correlation versus time. The slope of a linear curve fit through this data is the velocity of peak correlation, the magnitude of which is 182 m/s. As will be discussed, it is premature at this point to call this the convective velocity of structures in the flow. A dotted line shows the path that a structure would take if it were moving at the theoretically determined convective velocity of 296 m/s. Figure 8 d) is a histogram of the instantaneously determined values of the peak correlation velocity. The instantaneous values were determined by charting the location of maximum correlation for each image sequence independently. There are a few measurements near the theoretical value, indicated by the vertical line. Rather, the velocity is evenly distributed in two groups at ~175 m/s and 375 m/s.

Overall, the general nature of these results is very similar to the Mach 2.0 data presented in Thurow et al. [2003] and obtained using the same nozzle and similar experimental set-up. Earlier, this data was interpreted as demonstrating both a fast and a slow mode of convective velocity. As will be seen in the velocity data presented next, however, this may not have been the proper interpretation.

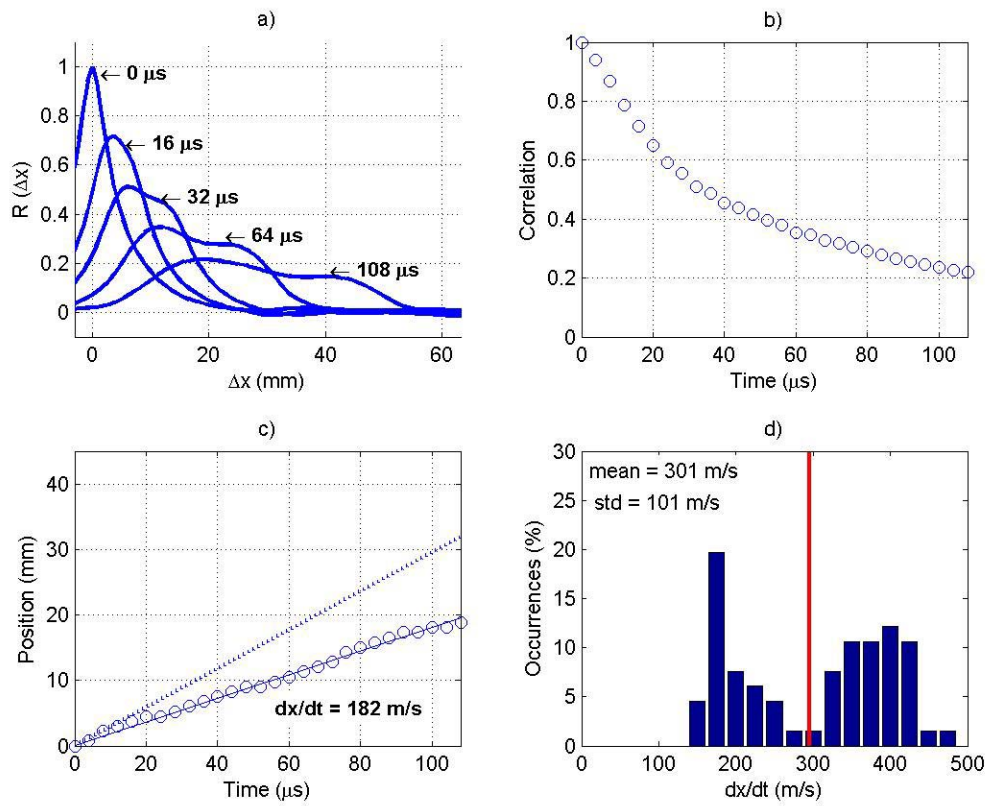

Figure 8: Two-dimensional space-time correlation results for Mach 2.0 flow visualization data a) Streamwise slice at t = 0, 16, 32, 64 and 108 μs; b) Peak correlation vs. time; c) Position of peak correlation vs. time; and d) Histogram of instantaneous convective velocity.

C. Velocity Data Space-Time Correlations

Figure 9 shows the space-time correlations for the seeded Mach 2.0 jet with all unseeded regions of the flow being set to a velocity of 0 m/s (1st method). The spatial correlations in Figure 9a) are slightly askew in the upstream direction, but do not exhibit any signs of a second peak, as observed in the flow visualization data. The x-t diagram (Figure 9c) shows the peak correlation moving with a velocity at 240 m/s, which is slower than the theoretical convective velocity, but with a much less severe deviation than that observed using the flow visualization (182 m/s). The histogram (Figure 9d) also does not show any indication of a bimodal distribution of convective velocities. Rather, the distribution is rather well centered near 250 m/s.

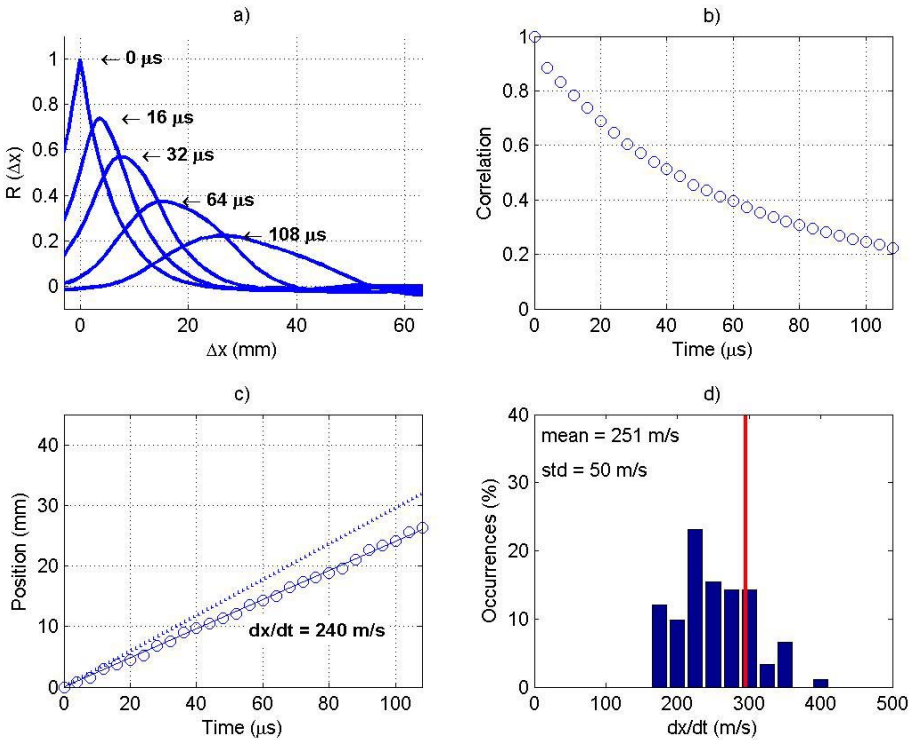

Figure 9: Two-dimensional space-time correlation results for Mach 2.0 jet velocity data with seeded jet core (no extrapolation) a) Streamwise slice at t = 0, 16, 32, 64 and 108 µs; b) Peak correlation vs. time; c) Position of peak correlation vs. time; and d) Histogram of instantaneous convective velocity.

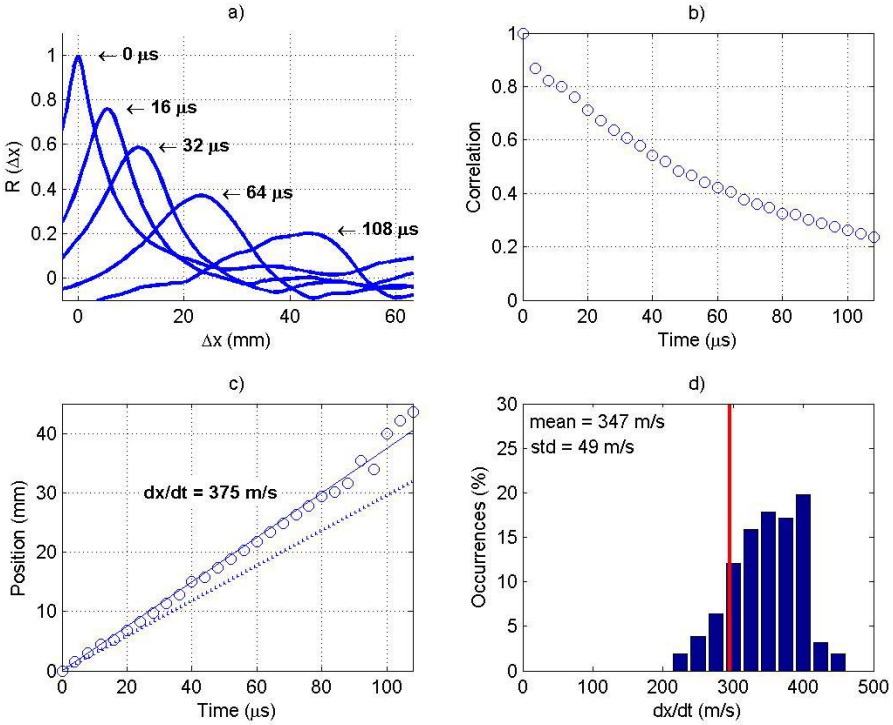

Figure 10: Two-dimensional space-time correlation results for Mach 2.0 jet velocity data with seeded jet core calculated using only non-zero values of velocity a) Streamwise slice at t = 0, 16, 32, 64 and 108 µs; b) Peak correlation vs. time; c) Position of peak correlation vs. time; and d) Histogram of instantaneous convective velocity.

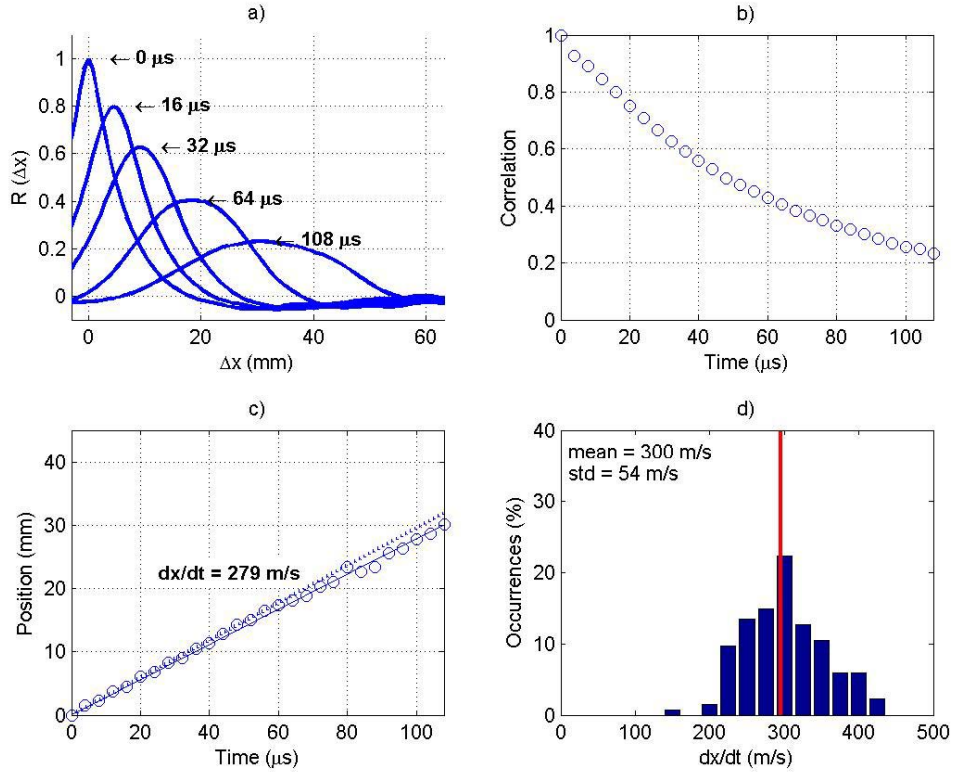

Figure 11: Two-dimensional space-time correlation results for Mach 2.0 jet velocity data with seeded jet core and near field values extrapolated a) Streamwise slice at t = 0, 16, 32, 64 and 108 µs; b) Peak correlation vs. time; c) Position of peak correlation vs. time; and d) Histogram of instantaneous convective velocity.

When only seeded regions of the flow are included in the calculation of the space-time correlation, the results are quite different. This is shown in Figure 10. The spatial correlations (Figure 10a) are slightly askew in the downstream direction and do not show any hints of a second peak. Unlike the previous case, the spatial correlation develops with a fast moving peak that, at 375 m/s, is significantly higher than the theoretical convective velocity (Figure 10c). As previously mentioned, this result is expected to be biased towards higher velocities as the unseeded regions of the jet tend to be at lower velocities and are not included in this calculation.

As a compromise between these two extremes, an algorithm was used to extrapolate the known velocity data into the unseeded regions of the image. Figure 11 shows the space-time correlation results when an error function (Eqn. 2.11) is used for curve fitting. Similar results are observed for any of the six functions discussed earlier (Equations 2.10 – 2.15). As before, the peak correlation broadens, its magnitude decreases, and its position translates downstream with increasing time (Figure 11a). Unlike before, the shape of the spatial correlation is quite symmetrical, almost Gaussian, and does not show skewness in the upstream or downstream direction. The ensemble average correlation velocity is calculated to be 279 m/s, which is only ~6% less than the theoretically expected convective velocity (Figure 11c). Over the first 60 µs the peak correlation is even closer (within 2%) to the theoretical convective velocity. After approximately 60 µs, the velocity of peak correlation slows down somewhat. This may be a physical feature of the flow but is likely an artifact of the extrapolation algorithm. The histogram in Figure 11d) shows the same features that the ensemble average shows with a mean velocity very close to the theoretical convective velocity. The distribution is roughly Gaussian with a mean value of 300 m/s and standard deviation of 54 m/s. As with the average velocity and rms velocity fluctuations profiles, the extrapolated data produces results that lie roughly in the middle of the other two methods used to treat the unseeded regions of the flow.

Figure 12 shows the location of peak correlation vs. time when using each of the six different functions for curve fitting. For approximately the first 40 µs, the peak location is the same for all six functions and the correlation velocity follows the theoretical convective velocity to within 2%. For longer periods of time, the data begins to spread out with some functions shows a slightly faster velocity and other functions a slightly slower velocity. Overall, however, the general trend of single velocity of peak correlation that is close to the theoretical value of convective velocity is preserved.

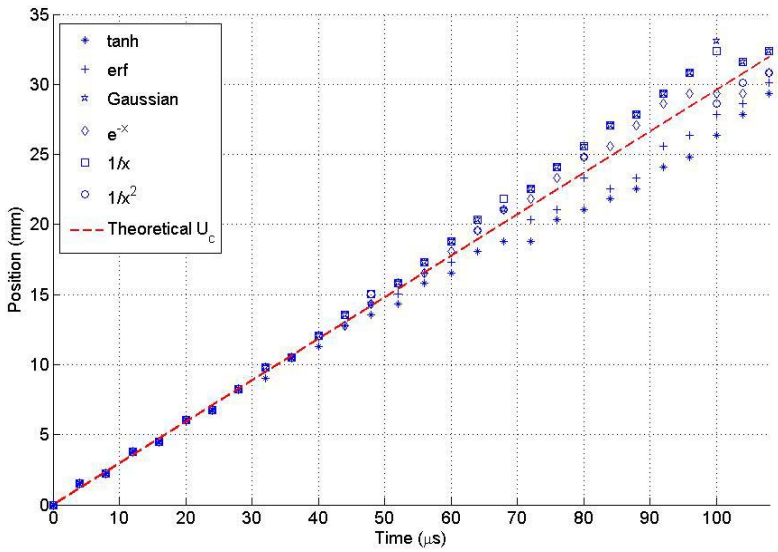

Figure 12 – Variation of location of peak correlation vs. time for six different functions used in the velocity extrapolation algorithm.

IV. Discussion of Results

The results presented in Section III are quite interesting, especially considering the number of researchers who have measured a deviation of the convective velocity based on flow visualization data. A discussion of these results is broken into three parts. First, an explanation is as to why flow visualization images can produce the misleading space-time correlations presented here. Second, the accuracy and validity of the convective velocity measurement based on the velocity data is discussed. Lastly, a brief discussion is provided concerning the implications that the current results have with respect to convective velocity measurements made by other researchers.

A. Bias of Flow Visualization Data

The purpose of the two-dimensional space-time correlation is to track structures as they convect downstream within the mixing layer. In this study, structures are defined by the signal (either intensity or velocity) contained within a pre-defined region of each image. For the calculation of convective velocity, one is most concerned with determining the location of peak correlation in space, Δx and Δy, at different instances in time. In this context, what are the defining features of a structure that will influence this determination? Consider a signal that varies significantly in space. In this case, the correlation level will be quite sensitive to the values of Δx and Δy as even a slight shift will cause a large mismatch between the two instances in time being compared. Conversely, consider a signal whose magnitude is relatively constant over its spatial dimensions. Increasing or decreasing Δx and Δy will have little effect on the correlation level as the signal does not exhibit much change. It logically follows then that the most distinguishing features of a structure will take the form of high spatial variations in the structure's signal.

Flow visualization images acquired using product formation for particle seeding are chiefly characterized by the boundary between mixed and unmixed fluid. Within regions of intense mixing (i.e. the center of a structure), the intensity is fairly constant. In regions with little to no mixing, condensation does not occur and the intensity level is approximately zero. The largest spatial gradients thus occur at the interface between mixed and unmixed fluid. These interfaces are the most defining features of the structures in the flow and it should be expected that the maximum spatial correlation will follow the location of this boundary. In the images examined here, there are two boundaries, one between the mixing layer and the high-speed side of the jet and the other between the mixing layer and the low-speed side of the jet.

It follows that space-time correlations of the flow visualization data will exhibit two convecting peaks, one associated with each boundary. This seems to adequately explain the observations made in the Mach 2.0 jet, where two modes of the velocity of peak correlation were observed. Should this imply that structures within the Mach 2.0

jet are moving at two different speeds? No! Rather, it is simply stating that the boundary between mixed and unmixed fluid (at least as defined via product formation) is moving at these two speeds. With this interpretation, these results are consistent with the one-dimensional correlation results of Samimy et al. (1992) and Elliott et al. (1995), which showed significant variation of convective velocity in the lateral direction (direction of shear).

B. Velocity Data

The most complete set of data produced in this study is the MHz rate PDV data of the Mach 2.0 jet with the jet core seeded using acetone condensation. The main deficiency of this data set, however, is that the ambient air is unseeded and no velocity information is available in the low-speed side of the mixing region. Three methods were used to treat these unseeded regions of the flow. In the first method, the velocity was set to zero if the pixel intensity registered below a set threshold level. In the second method, all of the space-time correlation equations were computed such that they only considered seeded regions of the flow. In the last method, an extrapolation algorithm was developed to approximate the velocity of the flow in these regions.

Space-time correlations using the first method show a velocity of the correlation peak of ~240 m/s, which is lower than the 296 m/s theoretical convective velocity. There is no sign of two modes of velocity and the magnitude of the deviation from theory is approximately half that measured using the flow visualization data. Considering the discussion above, it is clear that by treating unseeded regions of the flow as having zero velocity, a boundary, or spatial gradient, is created between the seeded and unseeded portions of the flow (in this case defined by velocity instead of intensity). This boundary is located on the low-speed side of the mixing layer and will have the effect of biasing the velocity of the correlation peak to low velocities as well.

As an alternative, the second method used a set of calculations for the correlation data where only data in the seeded regions of the flow were included. In this case, the velocity of the correlation peak (375 m/s) was higher than the theoretical convective velocity. At first glance, one might expect this result to be reasonable as it is not affected by the presence of an artificially imposed boundary. This result, however, is also biased by the fact that large regions of the flow are being ignored. In this case, the integration is not performed over the entire extent of the mixing layer, but is preferentially restricted to the high-speed side of the mixing layer. As the integration will include more data from the high-speed side than the low-speed side, it is expected that this data is biased towards higher velocities.

As a compromise to these two cases, the third method provides an approximation for the missing velocity data using a curve fitting extrapolation algorithm to determine the velocity in the unseeded regions of the flow. Six different functions were used for the curve fitting and the convective velocity was found to range from 270 to 310 m/s depending on which function was used and how many points were included from the x-t diagram in the calculation. Using only the first 60 μs (16 pts) of data, the convective velocity calculations only varied from 282 to 306 m/s, which are all within 5% of the theoretically expected value of 296 m/s. The fact that the results are similar for all six functions lends support to the idea that the extrapolation algorithm does a fair job at estimating the unmeasured portion of the flow. This would lead to the preliminary conclusion that the convective velocity of structures follows theoretical prediction for convective Mach numbers at least up to 0.87.

Unfortunately, not enough information is available at the present time to make this conclusion firm. In spite of the attractiveness of this idea, the data is still incomplete and could possibly be misinterpreted. More detailed studies are necessary to explore this issue. Modifications to the jet facility are currently being designed and developed that will allow for seeding of the entire flow field. These experiments will be conducted in the near future and should provide a more definitive answer concerning the convective velocity of structures in compressible flows.

C. Implications of Results

It is quite clear from the results presented here that, at the very least, the effects of compressibility on the convective velocity of large-scale structures needs to be reexamined. As discussed earlier, a large number of researchers (including this author) have measured a significant deviation of the convective velocity from its theoretically expected value with increasing compressibility levels. The common trait among all of these works is that the measurements are based on inherently qualitative flow visualization data. It is clearly shown here, however, that convective velocity measurements based on flow visualization data can be quite misleading. This is not to say that the measurements are in error, but, rather, that they could be misinterpreted. The inherent assumption in all of these works is that the flow visualization images capture the full extent of the large-scale structures. In reality, however, the techniques used by different researchers vary widely and each possesses its own unique set of characteristics that may affect the ability to visualize a large-scale structure. A comprehensive analysis of each of

these works is beyond the scope of this paper; however, a brief discussion is provided here concerning a small selection of works that have dealt with convective velocity measurements.

In a similar fashion to the current work, Fourgette et al. [1991] and Thurow et al. [2003] used planar laser Mie scattering for flow visualization and product formation for particle seeding to examine axisymmetric jets. Only a single fast mode was observed in the Mach 1.5 jet (M_c=0.7) of Fourgette et al. [1991] and the Mach 1.3 jet (M_c=0.59) in Thurow et al. [2003]. The flow visualization images from these works, however, are similar to the Mach 2.0 jet presented here and defined by both a high-speed and low-speed boundary. Based on the analysis given here, it would be expected that two modes of correlation velocity be observed, one for each boundary. Discussed in more detail in Thurow [2005], the reasons for the absence of a second mode are believed to lie in the nature of the product formation technique. Product formation is a complex process where moist ambient air must be entrained into the jet, mixed with cold, high-speed jet core fluid and its temperature reduced to allow condensation. In addition, these conditions must be met for a long enough time period for the water particles to grow to a large enough size to scatter detectable amounts of laser light. The Mach 2.0 jet, with an exit temperature of 155 K is ideal for this process as less fluid has to be mixed to achieve the necessary temperatures for condensation to occur. This allows for product formation to consistently happen throughout the entire mixing layer. In the Mach 1.3 jet of Thurow et al. [2003] and the Mach 1.5 jet of Fourgette et al. [1991], however, the jet exit temperature is warmer and more mixing must occur between the ambient air and the jet core for optimal product formation conditions to be met. Near the outer edge of the mixing layer, where the temperature will be higher, the product formation process is somewhat inhibited. It is conceivable then, that the boundary between the ambient air and the mixing layer will not be as distinct as the boundary between the jet core and the mixing layer, thus, the high-speed boundary yield higher correlations than the low-speed boundary. This idea is supported by average and rms fluctuating flow visualization images of the Mach 1.3 jet not included here, but presented in Thurow [2005].

An additional item that must be considered when analyzing these results is the role that compressibility has on the nature of structures contained in the flow, especially in contrast to the more familiar incompressible cases. At higher Reynolds number and compressibility levels, large-scale structures become less robust, less organized and less coherent. In addition, they may not span the entire mixing layer, which now contains a multitude of structures at a wide variety of scales. While still large, they occupy a portion of the mixing layer and can convect at different speeds according to their location. From the standpoint of space-time correlations, this means that the correlation will not be following a single well-defined structure that occupies the entire mixing layer. Rather, the correlation will 'see' the presence of many large-scale structures, varying in size, location and velocity. Without additional details (such as velocity), it is not clear how this will be reflected in the flow visualization data. The boundaries observed in the flow visualization images will be defined by these various structures and the nature of these structures may help distinguish one boundary from the other.

Elliott et al. [1995] also used product formation and Mie scattering flow visualization to determine a convective velocity. Unlike the other works, however, the space-time correlation was one-dimensional in space. They tracked a vertical line in the first image and computed its correlation at different streamwise and transverse locations in the second image. Interestingly, their data showed two correlation peaks at both M_c=0.51 and M_c=0.86. Because the correlation only considered a vertical line, these peak correlations were located at transverse locations away from the center of the mixing layer. The location of maximum correlation along the center of the mixing layer produced a convective velocity roughly equal to the theoretically expected value. This led them to conclude that the convective velocity varied with transverse location. More attention was not given to these results, however, as it was not clear that a vertical line contained enough information to truly represent a two- (actually three-) dimensional structure.

Papamoschou and Bunyajitradulya [1997] and Murakami and Papamoschou [2000] used planar laser-induced fluorescence (PLIF) to make measurements in supersonic shear layers and jets, respectively. In this technique, either the high or low-speed stream is seeded with gaseous acetone molecules which will fluoresce when illuminated with the fourth harmonic output (266 nm) of an Nd:YAG laser. Images produced using this technique display a boundary between the seeded flow and the unseeded flow with image intensity roughly corresponding to acetone density. While the size, shape and location of the boundary will be influenced by the underlying large-scale structures in the shear layer, it is probably not correct to assume that the boundary fully defines the large-scales structures. Rather, the location of the boundary may preferentially be closer to the high- or low-speed stream depending on the particular conditions of the experiment, thus yielding either a fast or slow mode of convective velocity.

It is interesting that for the nearly incompressible shear layer case (M_c=0.22) of Papamoschou and Bunyajitradulya [1997], the calculated convective velocity is quite close to the theoretical value, a result that the researchers used to validate their measurement. An alternative explanation, however, may be that compressibility alters the flow visualization process as opposed to the convective velocity. If the entire flow were uniformly seeded

with acetone, the intensity of the images would be proportional to the density of the flow. In this case, however, only one stream is seeded with acetone and the intensity of the images will be a function of both the flow density as well as the amount of mixing between the seeded and unseeded stream. For incompressible conditions, the flow density will not significantly change and the largest spatial gradient (or boundary) in the image will occur at the center of the mixing layer. Thus, the boundary will propagate at a value near the theoretically expected value. In a compressible flow, however, the mixing process will be accompanied by a change in flow density as well. It is conceivable that this process would lead to formation of large spatial gradients of intensity within the mixing layer that are offset from the center of structures contained in the mixing layer. This, of course, would lead to a bias in convective velocity measurements based on these visualizations. In a similar fashion, other flow visualization techniques should also be examined to determine how they might influence the ability to measure the convective velocity.

An additional method for determining the convective velocity of structures was employed by Hall et al. [1993] and Rossman et al. [2000] who based their measurements on the angle of emitted shock waves from structures in compressible shear layers. They used schlieren imaging to detect and measure the shock waves. For this to yield an accurate measurement of the convective velocity of large-scale structures, it must inherently be assumed that the shock wave is emitted from the center of the structure where the flow velocity would be equal to the convective velocity. The velocity within a structure will vary with transverse position and the formation of a shock within or in front of a large-scale structure is quite unclear and not well studied. Thus, it is not clear that the shock waves will directly correlate to the convective velocity of a structure. This is an interesting area worthy of more attention.

In all previous measurements, the presence of large-scale structures was inferred from the measurement of another, complex parameter (e.g. presence of shock waves, onset of product formation, etc.). It is clearly shown here that subsequently using this information to determine the convective velocity of the structure can be quite misleading. Our ability to extract further information beyond a qualitative assessment of the flow will inherently be limited by our lack of knowledge about the process that revealed the structure in the first place. While flow visualization is a powerful tool useful for making qualitative observations concerning the nature of a wide variety of flows, it cannot be forgotten that it is still inherently qualitative.

V. Conclusions

MHz rate PDV was used to make both flow visualization and velocity measurements of a Mach 2.0 compressible axisymmetric jet. Space-time correlations of both the flow visualization and velocity data revealed that the nature of the data has a strong influence on the ability of the space-time correlation to track structures in the flow. The flow visualization images of this study are marked by two well defined boundaries between mixed and unmixed fluid. The space-time correlation was found to follow these boundaries as opposed to the structure as a whole. Velocity measurements, although inherently more detailed, were also biased by the lack of seed particles in the ambient air. This necessitated the use of an extrapolation algorithm to approximate the velocity in unseeded regions of the flow.

Preliminary results based on the extrapolated velocity data seem to indicate that structures convect at the theoretical value of convective velocity. This is in stark contrast to convective velocity measurements based on flow visualization data. The implications of this are substantial as numerous researchers have made convective velocity measurements in the past based on flow visualization data. A few examples were given of how the past application of space-time correlations to flow visualization data could have produced misleading results concerning the convective velocity of structures. Overall, this work clearly illustrates the need for more detailed studies of compressibility effects on the dynamics of large-scale structures and marks substantial progress towards this goal of understanding. The MHz rate PDV system used for the measurements in this work will be used extensively in the near future to make further progress.

Acknowledgments

This research was supported in part through grants provided by the National Science Foundation, the Air Force Office of Scientific Research, and the Ohio Center for Advanced Propulsion and Power. The first author would like to acknowledge the support received as a National Defense Science and Engineering Graduate Fellow. The assistance of Naibo Jiang in the conducting of these experiments is greatly appreciated.

References

Bogdanoff, D. W., "Compressibility effects in turbulent shear layers," AIAA J., Vol. 21, 926, (1983).

Clancy, P.S., Samimy, M., and Erskine, W.R., "Planar Doppler Velocimetry: Three-Component Velocimetry in Supersonic Jets," *AIAA J.*, Vol. 37, 700, (1999).

Clemens, N. T. and Mungal, M. G., "Large-scale structure and entrainment in the supersonic mixing layer," J. Fluid Mech., Vol. 284, 171, (1995).

Crawford, J. B. and Elliott, G. S., "Multiple laser excitation for enhancement of large scale structures," AIAA Paper 99-0998, (1999).

Elliott, G. S., Samimy, M., and Arnette, S. A., "The characteristics and evolution of large-scale structures in compressible mixing layers," Phys. Fluids, Vol. 7, 864, (1995).

Elliott, G. S. and Beutner, T. J., "Molecular filter based planar Doppler velocimetry," *Progress in Aerospace Sciences*, Vol. 35, 799, (1999).

Fourgette, D. C., Mungal, M. G., and Dibble, R. W., "Time evolution of the shear layer of a supersonic axisymmetric jet," AIAA J., Vol. 29**,** 1123, (1991).

Goebel, S. G. and Dutton, J. C., "Velocity measurements of compressible, turbulent mixing layers," AIAA Paper 90-0709, (1990).

Hall, J. L., Dimotakis, P. E. and Rosemann, H., "Experiments in nonreacting compressible shear layers," AIAA J., Vol. 31, (1993).

Hileman, J. and Samimy, M., "Turbulence structures and the acoustic far field of a Mach 1.3 jet," *AIAA J.*, Vol. 39, 1716, (2001).

Kerechanin, C., Samimy, M., and Kim, J.-H., "Effects of nozzle trailing edge modifications on the far-field acoustic radiation in supersonic jets," *AIAA J.*, Vol. 39, 1065, (2001).

Lepicovsky, R., Ahuja, K.K., Brown, W.H., and Burrin R.H., "Coherent large-scale structures in high Reynolds number supersonic jets," *AIAA J.*, Vol. 25, 1419, (1987).

Mahadevan, R., Loth, E., and Dutton, J., "Effect of an expansion-compression wave pair on free shear layer dynamics," AIAA Paper 95-0475, (1995).

Murakami, E. and Papamoschou, D., "Eddy convection in coaxial supersonic jets," AIAA J. Vol. 38, 628, (2000).

Papamoschou, D. and Roshko, A., "The compressible turbulent shear layer: An experimental study," J. Fluid Mech., Vol. 197, 453, (1988).

Papamoschou, D., "Thrust loss due to supersonic mixing," AIAA J. Prop. Power, Vol. 10, 804, (1994).

Papamoschou, D. and Bunyajitradulya, "Evolution of large eddies in compressible shear layers," Phys. Fluids Vol. 9, 756, (1997).

Poggie, J. and Smits, A. J., "Large-scale coherent turbulence structures in a compressible mixing layer flow," AIAA Paper 96-0436, (1996).

Rossman, T., Mungal, M. G., and Hanson, R. K., "An experimental investigation of high compressibility non-reacting mixing layers," AIAA Paper 2000-0663, (2000).

Samimy, M. and Elliott, G. S., "Effects of compressibility on the characteristics of free shear layers," AIAA J., Vol. 28, 439, (1990).

Samimy, M., Reeder, M. F., and Elliott, G. S., "Compressibility effects on large structures in free shear flows," Phys. Fluids, Vol. 4, 1251, (1992).

Samimy, M., and Wernet, M.P., "Review of planar multiple-component velocimetry in high-speed flows," *AIAA J.,* Vol. 38, 553, (2000).

Smith, K. M. and Dutton, J. C., "Evolution and convection of large-scale structures in supersonic reattaching shear flows," Phys. Fluids, Vol. 11, 2127, (1999).

Thurow, B., Hileman, J., Lempert, W., and Samimy, M., "A technique for real-time visualization of flow structure in high-speed flows," Phys. Fluids, Vol. 14, 3449, (2002).

Thurow, B., Samimy, M., and Lempert, W., "Compressibility effects on turbulence structures of axisymmetric mixing layers," Phys. Fluids, Vol. 15, 1755, (2003).

Thurow, B., Jiang, N., Samimy, M., and Lempert, W., "Narrow-linewidth megahertz-rate pulse-burst laser for high-speed flow diagnostics," App. Opt., Vol. 43, 5064, (2004).

Thurow, B., Jiang, N., Lempert, W., and Samimy, M., "Development of megahertz-rate planar Doppler velocimetry for high-speed flows," AIAA J., scheduled to appear in 2005.

Thurow, B. "On the convective velocity of large-scale structures in compressible axisymmetric jets," Ph. D. Dissertation, The Ohio State University, 2005.